Modeling and control of a 4-wheel skid-steering mobile robot: From theory to practice*

K. Kozłowski[1], **D. Pazderski**[2]
Poznań University of Technology
ul. Piotrowo 3a
60-395 Poznań, Poland
[1]Krzysztof.Kozlowski@put.poznan.pl
[2]Dariusz.Pazderski@put.poznan.pl

I.Rudas[3], **J.Tar**[4]
Budapest Polytechnic
Népszínház utca 8.
H-1081 Budapest, Hungary
[3]rudas@bmf.hu
[4]tar.jozsef@nik.bmf.hu

Abstract:
In this paper problem of modeling and control of 4-wheel skid-steering mobile robot is presented. To obtain practical stabilization for both admissible and non-admissible trajectories [13, 7, 8], i.e. trajectories which do not satisfy nonholonomic constraint, control scheme which is based on kinematic algorithm [4, 5] is proposed. Theoretical considerations are verified by numerical simulation and experiments. In addition some details concerning implementation of proposed algorithm is given.

1 Introduction

Skid-steering mobile robots (SSMRs) are quite different from classical wheeled mobile robots for which lack of slippage is usually supposed – see for example [3]. In addition interaction between ground and wheels makes their mathematical model to be uncertain and caused control problem to be difficult as it generally demands quite detailed consideration of dynamic properties.

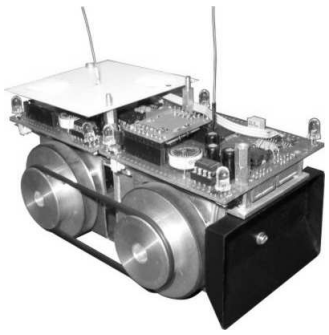

Figure 1: Experimental skid-steering mobile robot

In this paper we propose to use a continuous and time-differentiable control law which is based on kinematic oscillator [5] to resolve both regulation and trajectory tracking problem. Here we refer to work done by Caracciolo *et al.* [2] and our previous research which can be found in [10, 13]. To illustrate performance of the controller numerical simu-

*This research was supported by the Polish-Hungarian Bilateral Technology Co-operation Project and statuary grant No. DS 93/121/04 of Poznan University of Technology.

lations are presented. Next, experimental verification using small four-wheel SSMR (see Fig. 1) is described and some results of experiments are given.

2 Model of the robot

2.1 Introduction

In this section kinematic and dynamic model of four-wheel skid-steering mobile robot is presented. We refer to the real experimental construction consists of two-wheel differentially driven mobile robots namely MiniTracker 3 (see Fig.1) [9].

In order to simplify the mathematical model of SSMR we assume that [2]

- plane motion is considered only,
- achievable linear and angular velocities of the robot are relatively small,
- wheel contacts with surface at geometrical point (tire deformation is neglected),
- vertical forces acting on wheels are statically dependent on weight of the vehicle,
- viscous friction phenomenon is assumed to be negligible.

2.2 Kinematics

Firstly, consider a vehicle moving on two dimensional plane with inertial coordinate frame (X_g, Y_g) as depicted in Fig. 1(a). To describe motion of the robot it is convenient to define an local frame attached to it with origin in its center of mass (COM). Assume that $\boldsymbol{q} \triangleq \begin{bmatrix} X & Y & \theta \end{bmatrix}^T \in \mathbb{R}^3$ denotes generalized coordinates, where X, Y determine COM position and θ is an orientation the local frame with respect to the inertial frame, respectively.

Let $\boldsymbol{v} \triangleq \begin{bmatrix} v_x & v_y \end{bmatrix}^T \in \mathbb{R}^2$ be a velocity vector of COM expressed in the local frame with v_x and v_y determining longitudinal and lateral velocity of the vehicle [4].

From Fig. 1(a) it is easy to derive kinematic equation of motion using rotation matrix as follows

$$\dot{\boldsymbol{q}} = \begin{bmatrix} \dot{X} \\ \dot{Y} \\ \dot{\theta} \end{bmatrix} = \begin{bmatrix} \cos\theta & -\sin\theta & 0 \\ \sin\theta & \cos\theta & 0 \\ 0 & 0 & 1 \end{bmatrix} \begin{bmatrix} v_x \\ v_y \\ \omega \end{bmatrix}, \tag{1}$$

where $\dot{\boldsymbol{q}} \in \mathbb{R}^3$ is the generalized velocity vector and ω denotes angular velocity of the vehicle.

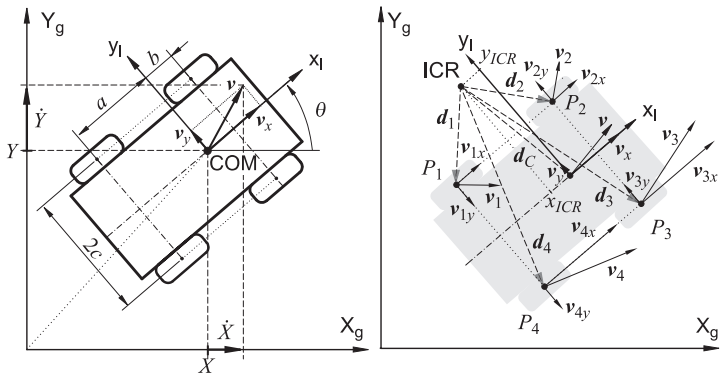

(a) Free-body kinematics

(b) Wheel velocities relationships

Figure 2: Kinematics of SSMR

To complete kinematic model of SSMR additional velocity constraints should be considered with respect to the inertial frame. According to geometrical situation presented in Fig. 1(b) one can prove that coordinates of velocities of points P_1, P_2,...,P_4 where the wheels of the robot touch the plane must satisfy [13, 12]

$$\begin{aligned} v_L &\triangleq v_{1x} = v_{2x}, \quad v_R \triangleq v_{3x} = v_{4x}, \\ v_F &\triangleq v_{2y} = v_{3y}, \quad v_B \triangleq v_{1y} = v_{4y}, \end{aligned} \tag{2}$$

where v_L, v_R denote longitudinal coordinates of left and right wheel velocities, v_F and v_B, are lateral coordinates of velocities of front and rear wheels, respectively.

Remark 1 *From Fig. 1(b) it is clear [13, 12] that v_{iy} is equal to zero for straight motion only (i.e. if $\omega = 0$), otherwise $v_{iy} \neq 0$ that implies lateral skid that is necessary to change orientation of such vehicle.*

Notice that ω_L and ω_R which denote angular velocities of left and right wheels, respectively, can be regarded as control inputs at kinematic level and can be used to control longitudinal and angular velocity according to the following relationships

$$v_x = r\frac{\omega_L + \omega_R}{2}, \quad \omega = r\frac{-\omega_L + \omega_R}{2c}, \tag{3}$$

while r is so called effective radius of wheels [11] and $2c$ is a spacing wheel track depicted in Fig. 1(a).

Remark 2 *It is very important to note that equations (3) are valid only if longitudinal slip does not appear, otherwise they should be treated as just approximations and to improve accuracy parameters c and r should be identified experimentally.*

Next, lateral velocity v_y which determines velocity of lateral slip of the vehicle can be obtained as follows [13]

$$v_y + x_{ICR}\omega = 0, \tag{4}$$

where x_{ICR} is a coordinate of instantaneous center of rotation (ICR) of the robot expressed along x_l axis. It can be proved that this equation in not integrable, hence it describes nonholonomic constraint and can be written in Pfaffian form as

$$\left[\begin{array}{ccc} -\sin\theta & \cos\theta & x_{ICR} \end{array} \right] \left[\begin{array}{ccc} \dot{X} & \dot{Y} & \dot{\theta} \end{array} \right]^T = \boldsymbol{A}\left(\boldsymbol{q}\right)\dot{\boldsymbol{q}} = \boldsymbol{0}, \tag{5}$$

where equation (1) has been used. Since the generalized velocity $\dot{\boldsymbol{q}}$ is always in the null space of $\boldsymbol{A}$ one can write that

$$\dot{\boldsymbol{q}} = \boldsymbol{S}\left(\boldsymbol{q}\right)\boldsymbol{\eta}, \tag{6}$$

where $\boldsymbol{\eta} \in \mathbb{R}^2$ is a control input at kinematic level defined as

$$\boldsymbol{\eta} \triangleq \left[\begin{array}{cc} v_x & \omega \end{array} \right]^T, \tag{7}$$

$\boldsymbol{S} \in \mathbb{R}^{3\times 2}$ is the following matrix

$$\boldsymbol{S}\left(\boldsymbol{q}\right) = \left[\begin{array}{cc} \cos\theta & x_{ICR}\sin\theta \\ \sin\theta & -x_{ICR}\cos\theta \\ 0 & 1 \end{array} \right] \tag{8}$$

which satisfies

$$\boldsymbol{S}^T\left(\boldsymbol{q}\right)\boldsymbol{A}^T\left(\boldsymbol{q}\right) = \boldsymbol{0}. \tag{9}$$

Remark 3 *Equation (6) describes kinematics of SSMR which will be used to formulate control law. Since $dim\left(\boldsymbol{\eta}\right) < dim\left(\boldsymbol{q}\right)$ SSMR can be regarded as an underactuated system. Furthermore, because of constraint (5) this system is nonholonomic.*

2.3 Dynamics

Because of interaction between wheels and ground dynamic properties of SSMR play a very important role. It should be noted that if the robot is changing its orientation reactive friction forces are usually much higher than forces resulting from inertia. As a consequence, even for relatively low velocities, dynamic properties of SSMR influence motion much more than for other vehicles for which non-slipping and pure rolling assumption may be satisfied.

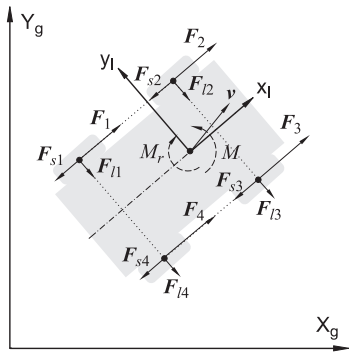

Figure 3: Forces and torques

However in this section only simplified dynamics of SSMR [2], which will be useful for control purpose, are introduced. In order to simplify this model we assume that the mass distribution of the vehicle is almost homogeneous, kinetic energy of the wheels and

drives can be neglected and detailed description of tyre which can be found, for example, in [11] are omitted.

A dynamic equation of SSMR can be obtained using Euler-Lagrange principle with Lagrange multipliers to include nonholonomic constraint and it can be written as

$$\boldsymbol{M}(\boldsymbol{q})\ddot{\boldsymbol{q}} + \boldsymbol{R}(\dot{\boldsymbol{q}}) = \boldsymbol{B}(\boldsymbol{q})\boldsymbol{\tau} + \boldsymbol{A}^T(\boldsymbol{q})\boldsymbol{\lambda}, \tag{10}$$

where $\boldsymbol{M} \in \mathbb{R}^{3\times 3}$ denotes the constant, diagonal, positive definite inertia matrix

$$\boldsymbol{M} = \begin{bmatrix} m & 0 & 0 \\ 0 & m & 0 \\ 0 & 0 & I \end{bmatrix}, \tag{11}$$

m, I represent the mass and inertia, respectively, $\boldsymbol{R}(\dot{\boldsymbol{q}}) \in \mathbb{R}^3$ denotes vector of resultant reactive forces F_l, F_s and torque M_r

$$\boldsymbol{R}(\dot{\boldsymbol{q}}) = \begin{bmatrix} F_s(\dot{\boldsymbol{q}})\cos\theta - F_l(\dot{\boldsymbol{q}})\sin\theta \\ F_s(\dot{\boldsymbol{q}})\sin\theta + F_l(\dot{\boldsymbol{q}})\cos\theta \\ M_r(\dot{\boldsymbol{q}}) \end{bmatrix}, \tag{12}$$

$\boldsymbol{B} \in \mathbb{R}^{3\times 2}$ denotes input matrix and is explicitly defined as follows

$$\boldsymbol{B}(\boldsymbol{q}) = \frac{1}{r}\begin{bmatrix} \cos\theta & \cos\theta \\ \sin\theta & \sin\theta \\ -c & c \end{bmatrix}. \tag{13}$$

The term $\boldsymbol{\tau} = \begin{bmatrix} \tau_L & \tau_R \end{bmatrix}^T \in \mathbb{R}^2$ which appears in (10) can be treated as a control signal at dynamic level and represents torques generated by actuators on the left and right side of the robot. Notice that these torques produce active forces F_i (see Fig. 3) that are theoretically independent on longitudinal slip.

The reactive forces and torque in (12) are calculated as

$$F_s(\dot{\boldsymbol{q}}) = \sum_{i=1}^{4} F_{si}(\dot{\boldsymbol{q}}), \quad F_l(\dot{\boldsymbol{q}}) = \sum_{i=1}^{4} F_{li}(\dot{\boldsymbol{q}}) \tag{14}$$

and

$$\begin{aligned} M_r(\dot{\boldsymbol{q}}) &= b\left[F_{l2}(\dot{\boldsymbol{q}}) + F_{l3}(\dot{\boldsymbol{q}})\right] - a\left[F_{l1}(\dot{\boldsymbol{q}}) + F_{l4}(\dot{\boldsymbol{q}})\right] \\ &\quad + c\left[-F_{s1}(\dot{\boldsymbol{q}}) - F_{s2}(\dot{\boldsymbol{q}}) + F_{s3}(\dot{\boldsymbol{q}}) + F_{s4}(\dot{\boldsymbol{q}})\right] \end{aligned} \tag{15}$$

where

$$F_{si}(\dot{\boldsymbol{q}}) \triangleq \mu_{si} N_i \operatorname{sgn}(v_{ix}), \quad F_{li}(\dot{\boldsymbol{q}}) \triangleq \mu_{li} N_i \operatorname{sgn}(v_{iy}) \tag{16}$$

while μ_{si} and μ_{li} are dry friction coefficients for i^{th} wheel in longitudinal and lateral direction, respectively, N_i is a reactive vertical force which acts on wheel and is supposed to be statically dependent on weight of the vehicle (see [2]).

For control purpose it would be convenient to express dynamic equation in $\boldsymbol{\eta}$ and $\dot{\boldsymbol{\eta}}$ terms. According to it one can obtain that

$$\bar{\boldsymbol{M}}\dot{\boldsymbol{\eta}} + \bar{\boldsymbol{C}}\boldsymbol{\eta} + \bar{\boldsymbol{R}} = \bar{\boldsymbol{B}}\boldsymbol{\tau}, \tag{17}$$

where relationships (6) and (9) have been used,

$$\bar{\boldsymbol{M}} = \boldsymbol{S}^T\boldsymbol{M}\boldsymbol{S}, \quad \bar{\boldsymbol{C}} = \boldsymbol{S}^T\boldsymbol{M}\dot{\boldsymbol{S}}, \quad \bar{\boldsymbol{R}} = \boldsymbol{S}^T\boldsymbol{R}, \quad \bar{\boldsymbol{B}} = \boldsymbol{S}^T\boldsymbol{B}. \tag{18}$$

3 Controller

3.1 Operational constraint

In previous section the constraint (4) was considered. However it is difficult to measure or estimate x_{ICR} value in practice. Therefore motivated by work done by Caracciolo *et al.* [2] we put an artificial constraint based on (4) and assume that $x_{ICR} = x_0 = const$. It can be written as

$$v_y + x_0\omega = 0, \tag{19}$$

where $x_0 \in (-a, b)$, while a and b are geometrical parameters depicted in Fig. 1(a). This assumption is consequently used in control development and can be interpreted as an outer-loop term in the controller which limits skid of the vehicle in lateral direction [13].

3.2 Control objective

For control purposes the following tracking error is defined

$$\tilde{\boldsymbol{q}}(t) \triangleq \begin{bmatrix} \tilde{X}(t) & \tilde{Y}(t) & \tilde{\theta}(t) \end{bmatrix}^T = \boldsymbol{q}(t) - \boldsymbol{q}_r(t), \tag{20}$$

where $\boldsymbol{q}_r(t) = \begin{bmatrix} X_r(t) & Y_r(t) & \theta_r(t) \end{bmatrix}^T$ denotes reference position and orientation. We assume that for all times reference vector and its first and second time derivative are bounded, i.e. $\boldsymbol{q}_r(t), \dot{\boldsymbol{q}}_r(t), \ddot{\boldsymbol{q}}_r(t) \in \mathscr{L}_\infty$. Here we do not imposed any additional restriction on reference signal $\boldsymbol{q}_r$ (regulation case can be considered, too). Additionally, in opposite to the previous works [5, 4, 10, 13] we consider the case for which $\boldsymbol{q}_r$ is defined in a such way that velocities associated with it do not satisfy nonholonomic constraints.

In order to facilitate subsequent control we determine kinematic error assuming that the constraint (19) is satisfied. Next, taking the time derivative of equation (6) and using relationship (9) one can conclude that

$$\dot{\tilde{\boldsymbol{q}}}(t) = \boldsymbol{S}(\boldsymbol{q})\boldsymbol{\eta} - \dot{\boldsymbol{q}}_r(t). \tag{21}$$

3.3 Position and velocity transformations

Kinematic controller based on Dixon's scheme uses transformation which transforms original system – in this case described by equation (21) – to an auxiliary system (22) similar to nonholonomic Brockett's integrator [1]

$$\dot{w} = \boldsymbol{u}^T \boldsymbol{J}^T \boldsymbol{z} + f, \quad \dot{\boldsymbol{z}} = \boldsymbol{u}, \tag{22}$$

where variables $w \in \mathbb{R}^1$ and $\boldsymbol{z} \in \mathbb{R}^2$ form three-dimensional state vector, $\boldsymbol{u} \in \mathbb{R}^2$ is a new velocity control vector and $f \in \mathbb{R}^1$ is a drift of the system, while $\boldsymbol{J}$ represents a constant, skew symmetric matrix defined as

$$\boldsymbol{J} = \begin{bmatrix} 0 & -1 \\ 1 & 0 \end{bmatrix}. \tag{23}$$

It can be proved that following transformation defines global diffeomorphism with respect to the origin

$$\boldsymbol{Z} \triangleq \begin{bmatrix} w & \boldsymbol{z}^T \end{bmatrix}^T = \boldsymbol{P}\left(\theta, \tilde{\theta}\right) \tilde{\boldsymbol{q}}, \tag{24}$$

where

$$\boldsymbol{P}\left(\theta, \tilde{\theta}\right) = \begin{bmatrix} -\tilde{\theta}\cos\theta + 2\sin\theta & p_{12} = -\tilde{\theta}\sin\theta - 2\cos\theta & -2x_0 \\ 0 & 0 & 1 \\ \cos\theta & \sin\theta & 0 \end{bmatrix}. \tag{25}$$

Using this transformation and calculating auxiliary errors we can find velocity transformation which relates velocity vector $\boldsymbol{\eta}$ with control signal $\boldsymbol{u}$ as follows

$$\boldsymbol{\eta} = \boldsymbol{T}\left(\tilde{\boldsymbol{q}}, \boldsymbol{q}\right) \boldsymbol{u} + \boldsymbol{\Pi}, \tag{26}$$

where

$$\boldsymbol{T}\left(\tilde{\boldsymbol{q}}, \boldsymbol{q}\right) = \begin{bmatrix} L & 1 \\ 1 & 0 \end{bmatrix} \tag{27}$$

is an invertible velocity transformation matrix, $L = \tilde{X}\sin\theta - \tilde{Y}\cos\theta$ and

$$\boldsymbol{\Pi}\left(\boldsymbol{q}, \boldsymbol{q}_r, t\right) = \begin{bmatrix} \omega_r L + \dot{X}_r \cos\theta + \dot{Y}_r \sin\theta \\ \omega_r \end{bmatrix} \tag{28}$$

is a time-varying vector associated with reference trajectory. In the similar way we can calculate drift term f as follows

$$f = 2\left[\omega_r \left(x_0 + z_2 - \dot{X}_r \sin\theta + \dot{Y}_r \cos\theta\right)\right]. \tag{29}$$

Summarizing, the obtained velocity transformation allows to use kinematic controller to resolve practical stabilization for admissible and non-admissible trajectories.

3.4 Control law

In this paper we propose to resolve control at kinematic level using algorithm based on Dixon's research. The more details concerning this approach can be found in [5, 4, 13]. This controller allows to obtain practical stabilization [7], i.e. tracking error is bounded to the assumed non zero value. The actual desired tunnel of errors is determined by function $\delta_d(t) = \alpha_0 \exp(\alpha_1 t) + \varepsilon_1$, where $\alpha_0, \alpha_1 > 0$ are constant parameters and ε_1 denotes desired steady-state value of vector $\boldsymbol{z}$ norm. This function describes envelope of an additional signal $\boldsymbol{z}_d$ generated by tunable oscillator.

In order to extend kinematic algorithm at dynamic level a backstepping technique is used. Based on Lyapunov analysis we propose the following control law which is robust on dynamic parameter uncertainty

$$\boldsymbol{\tau} \triangleq \bar{\bar{\boldsymbol{B}}}^{-1} \left(w\boldsymbol{J}\boldsymbol{z} + \tilde{\boldsymbol{z}} + \boldsymbol{Y}_d \boldsymbol{\vartheta}_0 + \boldsymbol{\tau}_a + k_3 \tilde{\boldsymbol{u}} \right), \tag{30}$$

where $\boldsymbol{Y}_d(\boldsymbol{u}_d, \dot{\boldsymbol{u}}_d, \tilde{\boldsymbol{q}}, \theta, \boldsymbol{q}_r) \in \mathbb{R}^{2\times 6}$ represents known regression matrix as

$$\bar{\bar{\boldsymbol{M}}} \dot{\boldsymbol{u}}_d + \bar{\bar{\boldsymbol{C}}} \boldsymbol{u}_d + \bar{\bar{\boldsymbol{R}}} = \boldsymbol{Y}_d(\boldsymbol{u}_d, \dot{\boldsymbol{u}}_d, \tilde{\boldsymbol{q}}, \theta, \boldsymbol{q}_r)\, \boldsymbol{\vartheta}, \tag{31}$$

$$\begin{aligned} \bar{\bar{\boldsymbol{M}}} &= \boldsymbol{T}^T \bar{\boldsymbol{M}} \boldsymbol{T}, \quad \bar{\bar{\boldsymbol{C}}} = \boldsymbol{T}^T \left(\bar{\boldsymbol{C}} \boldsymbol{T} + \bar{\boldsymbol{M}} \dot{\boldsymbol{T}} \right), \\ \bar{\bar{\boldsymbol{R}}} &= \boldsymbol{T}^T \left(\bar{\boldsymbol{C}} \boldsymbol{\Pi} + \bar{\boldsymbol{M}} \dot{\boldsymbol{\Pi}} + \bar{\boldsymbol{R}} \right), \quad \bar{\bar{\boldsymbol{B}}} = \boldsymbol{T}^T \bar{\boldsymbol{B}}, \end{aligned} \tag{32}$$

with $k_3 > 0$, while $\boldsymbol{u}_d$ is a velocity control signal generated by kinematic controller (see [13]), $\boldsymbol{\vartheta}$ and $\boldsymbol{\vartheta}_0$ are actual and a constant, best-guess estimation of dynamical parameter vector, respectively. According to [14] and [5] the term $\boldsymbol{\tau}_a$ is defined as

$$\boldsymbol{\tau}_a \triangleq \boldsymbol{Y}_d \frac{\rho^2 \boldsymbol{Y}_d^T \tilde{\boldsymbol{u}}}{\left\| \boldsymbol{Y}_d^T \tilde{\boldsymbol{u}} \right\| \rho + \varepsilon_2}, \tag{33}$$

where ε_2 is a positive constant scalar which can be made arbitrary small. The dynamic parameters in (31) are determined as

$$\boldsymbol{\vartheta} \triangleq \begin{bmatrix} m & I & \mu_L & \mu_R & \mu_F & \mu_B \end{bmatrix}^T \in \mathbb{R}^6 \tag{34}$$

with weighted friction coefficients defined as

$$\begin{aligned} \mu_L &\triangleq \frac{b\mu_{s1} + a\mu_{s2}}{a+b}, \qquad \mu_R \triangleq \frac{b\mu_{s4} + a\mu_{s3}}{a+b} \\ \mu_F &\triangleq \frac{2a(\mu_{l2} + \mu_{l3})}{a+b}, \quad \mu_B \triangleq \frac{2b(\mu_{l1} + \mu_{l4})}{a+b} \end{aligned} \tag{35}$$

Remark 4 *It can be proved [10] that proposed kinematic control law and its extension at dynamic level ensures practical stabilization yielding ultimately bounded tracking error under assumptions that constraint (4) is satisfied, parameters uncertainty is limited and trajectory signals are bounded that has been pointed in section 3.2.*

4 Simulation results

In this section we present simulation results performed in Matlab/Simulink environment to verify behavior of the controller. The parameters of the SSMR model were chosen to correspond as closely as possible to the real experimental robot presented in section 1 in the following manner: $a = b = 0.039[m]$, $c = 0.034[m]$, $r = 0.0265[m]$, $m = 1[kg]$, $I = 0.0036[kg \cdot m^2]$.

Permissible torque signal and angular velocities of wheels were saturated as: $\tau_{max} = 0.25[Nm]$, $\omega_{max} = 56[rad/s]$. Friction parameters of the surface μ_{si} and μ_{li}were modeled using scalar functions depending on actual position of center of i^{th} wheel expressed in the inertial frame and were supposed to be bounded as follows: $0.02 \leq \mu_{si} \leq 0.18$, $0.2 \leq \mu_{li} \leq 0.8$.

Remark 5 *For comparison purpose initial conditions and the parameters assumed in simulations correspond to those used in experiments which are described in section 5.*

Firstly, regulation problem is examined. The initial posture error was selected as $\tilde{\boldsymbol{q}}(0) = \begin{bmatrix} 0 & 0.5 & -\pi/4 \end{bmatrix}^T$. The control gains were given as $k_1 = 0.5$, $k_2 = 0.5$, $k_3 = 10$, while coefficients which determine accuracy in steady-state were $\varepsilon_1 = 0.01$ and $\varepsilon_2 = 0.1$. The oscillator signal was initialized as follows

$$z_d(0) = 1.5 \begin{bmatrix} \cos(-\pi/3) & \sin(-\pi/3) \end{bmatrix}^T$$

and the coefficient which determines desired convergence of errors was selected as $\alpha_1 = 0.4$.

The best-guess estimates of mass and inertia were 20 and 50 percent higher, respectively, than parameters assumed for the robot model. Next, estimates of friction coefficients were selected as $\mu_{L0} = \mu_{R0} = 0.1$ and $\mu_{F0} = \mu_{B0} = 0.5$, while bounding coefficient $\rho = 1$. Furthermore, the constant x_0 related to ICR position was assumed to be equal to $-0.02\,[m]$.

In Fig. 3(a) performed trajectory in Cartesian space is depicted and the position and orientation is marked at every second of simulation. From Fig. 3(b) it is clear that initial errors are significant reduced and in steady-state are bounded as follows

$$\left|\tilde{X}\right| < 5[mm], \quad \left|\tilde{Y}\right| < 5[mm], \quad \left|\tilde{\theta}\right| < 0.01[rad].$$

It is worth to note that convergence to the set of permissible errors is exponential.

In the next simulation trajectory tracking were examined. The sinusoidal admissible reference trajectory were selected as

$$X_r = 0.1t\,[m], \quad Y_r = 0.3\sin(0.6t)\,[m],$$

while θ_r was numerically calculated to satisfy the constraint (19). The initial oscillator signal was selected as

$$z_d(0) = 0.4 \begin{bmatrix} \cos(-\pi/2) & \sin(-\pi/2) \end{bmatrix}^T$$

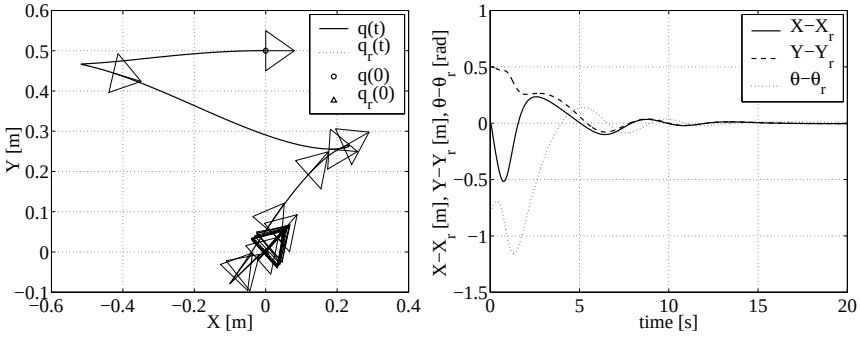

(a) Performed trajectory (b) Regulation errors

Figure 4: Regulation case

and the gain coefficient k_2 was increased to 1 in comparison to the previous simulation. Other parameters of the controller remained unchanged.

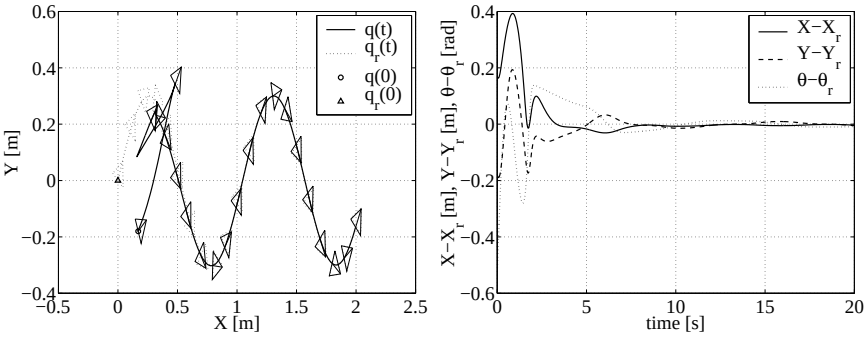

(a) Performed and reference trajectory (b) Regulation errors

Figure 5: Admissible trajectory case

The reference and performed trajectory are presented in Fig. 4(a) using stroboscopic view, while position and orientation errors are depicted in Fig. 4(b). These steady-state errors are bounded as

$$\left|\tilde{X}\right| < 10[mm], \quad \left|\tilde{Y}\right| < 10[mm], \quad \left|\tilde{\theta}\right| < 0.01[rad].$$

It should be noted that further error reduction in steady-state is possible by choosing smaller value ε_1. Next, convergence of errors may be improved by increasing value α_1. However, tuning of the controller parameters should take into consideration limitation of torque and velocity signals since forcing too small desired errors or too fast convergence may result in bad performance of the controller and may cause chattering phenomenon.

5 Experimental verification

5.1 Experimental setup

The experimental setup depicted in Fig. 6 consists of SSMR mobile robot built on the redesigned MiniTracker-3 robots and test board on which the robot moves. To localize the robot we were not able to use classical odometry system because of slip phenomena. Instead of it we used an external vision system [6] in the form of video camera SONY DCR-TRV900E and PC Pentium 4 1.6 GHz computer equipped with frame-grabber card Matrox CORONA which converts analog signal to digital signal. To inquire information about actual robot posture two-dimensional images were processed by software algorithm operated by the computer as they came from the camera. To simplify and improve recognition of the robot an additional color markers were placed on it.

The software has been written in C++ language and were performed under MS Windows 2000 system. The system synchronization was achieved by using frame-grabber card which allows to obtain 25 measurements per second. The communication between the robot and PC was ensured by radio link with throughput up to 115,2 kbit/s.

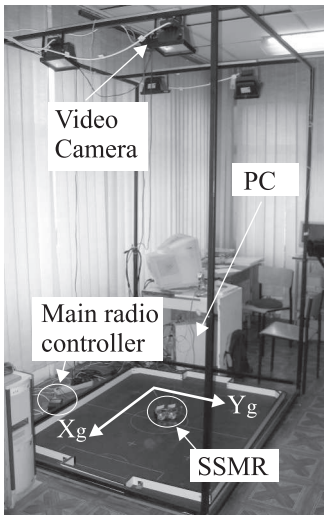

Figure 6: Experimental setup

The main drawback of used localization system lies in relatively small frequency of data acquisition (25 times per second) and small accuracy of determining orientation of the robot. As a consequence measurement of angular velocity were noisy and therefore it was no possible to implement robust control law presented in section 3.4.

Instead of it control task was divided between PC and internal controller of the experimental robot. Next, we modified the controller at kinematic level by calculating directly desired angular velocities ω_{dL} and ω_{dR} of the left and right wheels, respectively, according to (26) and (3) as follows

$$\begin{bmatrix} \omega_{dL} \\ \omega_{dR} \end{bmatrix} = \frac{1}{r} \begin{bmatrix} 1 & c \\ 1 & -c \end{bmatrix} \begin{bmatrix} 1 & 0 \\ 0 & -\frac{1}{x_0} \end{bmatrix} (\boldsymbol{T}\boldsymbol{u}_d + \boldsymbol{\Pi}), \tag{36}$$

where parameter c has been identified experimentally.

These signals determined by PC using actual posture measurement were sent to the robot using radio-link. The on-board PI controller working with frequency 512Hz controlled velocity of wheels using current forcing mode [9] that gives short transient phase during regulation process.

To calculate oscillator signal $\boldsymbol{z}_d$ trapezoidal integration routine was used. In addition to ensure numerical stability of the algorithm scaling operation was performed to stabilized envelope of $\|\boldsymbol{z}_d\|$ determined by function $\delta_d\,(t)$.

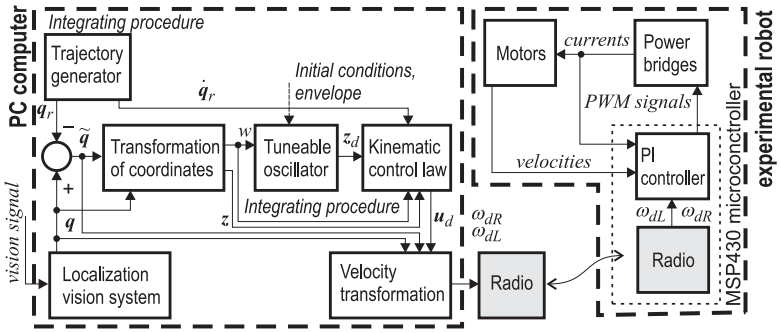

Figure 7: Controller diagram

Remark 6 *It should be noted that implemented control scheme is based on assumption that longitudinal slip is negligible. In theory this assumption would not be necessary for overall controller previously verified in simulation section.*

5.2 Results

To validate the proposed simplified algorithm results of experiments are presented.

Firstly, we considered the regulation problem, i.e. parking problem. The parameters of the controller and initial conditions were presented in section 4, however ε_1 was increased to 0.05 to ensure better robustness and less sensitiveness to measurement noise.

The results are depicted in Figs. 7(a)–7(b). From Fig. 7(a) one can see that steady-states position and orientation errors were bounded as follows

$$\left|\tilde{X}\right| < 20[mm], \quad \left|\tilde{Y}\right| < 20[mm], \quad \left|\tilde{\theta}\right| < 0.03[rad].$$

In the next experiment trajectory tracking was verified. The reference trajectory was the same as it used in simulation and the parameter ε_1 was selected as $\varepsilon_1 = 0.15$ to improve robustness of the controller. From Fig. 8(a) and 8(b) one can see that accuracy of tracking is significantly less than accuracy obtained for regulation that results mainly from unmodeled dynamic effects (for example slip phenomenon) and delays in the control loop. The tracking errors were bounded as

$$\left|\tilde{X}\right| < 80[mm], \quad \left|\tilde{Y}\right| < 180[mm], \quad \left|\tilde{\theta}\right| < 0.3[rad].$$

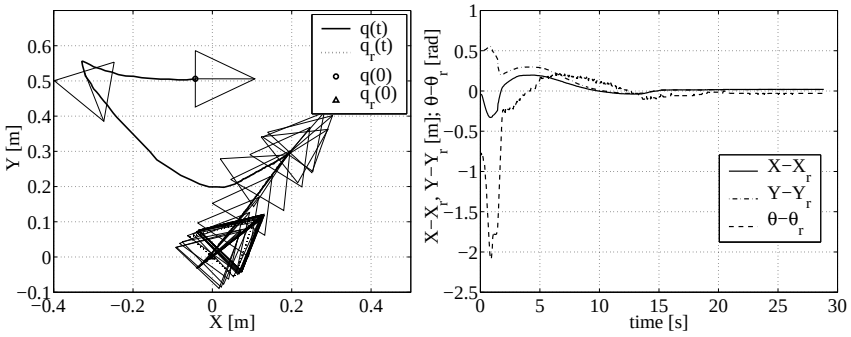

(a) Performed trajectory (b) Regulation errors

Figure 8: Experimental results – regulation case

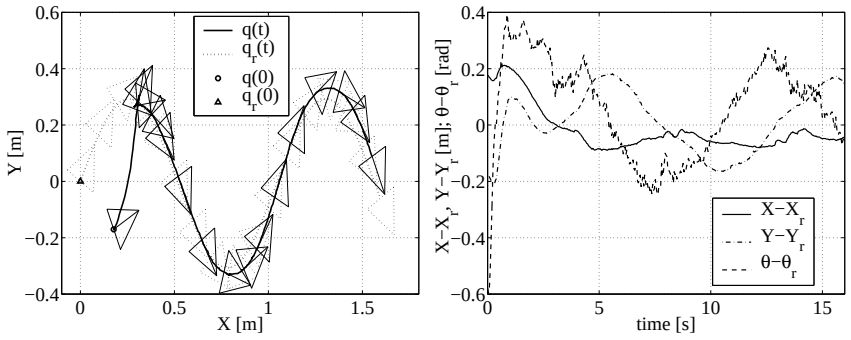

(a) Performed and reference trajectory (b) Tracking errors

Figure 9: Experimental results – trajectory tracking case

6 Summary

In this paper the control algorithm which resolves both trajectory tracking and regulation problem for 4-wheel skid-steering mobile robot is presented. In particular much attention is dedicated to show implementation and experimental results for the controller. We believe that further improvement of accuracy is possible by using a new measurement and localization system in form of monolithic optical sensors and accelerometers. It would allow to implement overall control scheme presented in theoretical description.

On the other hand it is worthy to note that SSMR is quite difficult to control that results from unmodeled dynamic effects, hence achieving small tracking errors may be impossible. Therefore the algorithms which ensure practical stabilization with good robustness on unmodeled phenomena can be very useful in practice [8].

References

[1] R. W. Brockett, "Asymptotic stability and feedback stabilization", *Differential Geometric Control Theory* edited by R. W. Brockett, R. S. Milman and H. J. Susmann, Birkhauser, Boston, pp. 181-191, 1983.

[2] L. Caracciolo, A. De Luca, S. Iannitti, "Trajectory tracking control of a four-wheel differentially driven mobile robot", *IEEE Int. Conf. on Robotics and Automation*, Detroit, MI, pp. 2632-2638, May 1999.

[3] G. Campion, G. Bastin, B. DAndrea-Novel, "Structural Properties and Classification of Kinematic and Dynamic Models of Wheeled Mobile Robots", *IEEE Transactions on Robotics and Automation*, Vol. 12, No.1, pp. 47-62, February 1996.

[4] W.E.Dixon, A.Behal, D.M.Dawson, S.P.Nagarkatti, *Nonlinear Control of Engineering Systems, A Lyapunov-Based Approach*, Birkhauser 2003.

[5] W. E. Dixon, D. M. Dawson, E. Zergeroglu and A. Behal, *Nonlinear Control of Wheeled Mobile Robots*, Springer-Verlag, 2001.

[6] P. Dutkiewicz, M. Kiełczewski, "Vision feedback in control of a group of mobile robots". Proc. of the *Seventh International Conference on Climbing and Walking Robots and their Supporting Technologies for Mobile Machines CLAWAR 2004*, Madrit 2004 (to appear).

[7] P. Morin, C. Samson, "Practical Stabilization of Driftless Systems on Lie Groups: The Transverse Function Approach", *IEEE Transactions on Automatic Control*, Vol. 48, No.9, pp.1496-1508, September 2003.

[8] P. Morin, C. Samson, "Feedback control of nonholonomic wheeled vehicles, A survey", *Archives of Control Sciences*, Vol. 12, pp.7-36, 2002.

[9] T. Jedwabny, M. Kowalski, M. Kiełczewski, M. Ławniczak, M. Michalski, M. Michałek, D. Pazderski, K. Kozłowski, Nonholonomic mobile robot MiniTracker 3 for research and educational purposes, 35^{th} International Symposium on Robotics, Paris 2004.

[10] K. Kozłowski, D. Pazderski, "Control of a Four-Wheel Vehicle Using Kinematic Oscillator". Proc. of the *Sixth International Conference on Climbing and Walking Robots and their Supporting Technologies CLAWAR 2003*, pp. 135-146, Catania 2003.

[11] H. B. Pacejka, *Tyre and Vehicle Dynamics*, Butterworth-Heinemann, 2002.

[12] D. Pazderski, K. Kozłowski, M. Ławniczak, "Practical stabilization of 4WD skid-steering mobile robot". Proc. of the *Fourth International Workshop on Robot Motion and Control*, Puszczykowo, pp. 175-180, 2004.

[13] D.Pazderski, K.Kozłowski, W.E.Dixon, "Tracking and Regulation Control of a Skid Steering Vehicle", *American Nuclear Society Tenth International Topical Meeting on Robotics and Remote Systems*, Gainesville, Florida, pp. 369-376, March 28-April 1 2004.

[14] M. W. Spong, "On the Robust Control of Robot Manipulators", *IEEE Transactions on Automatic Control*, Volume 37, No. 11, pp. 1782-1786, November 1992.